Journal of Alloys and Compounds 509 (2011) 5400–5407

Contents lists available at ScienceDirect

Journal of Alloys and Compounds

journal homepage: www.elsevier.com/locate/jallcom

Growth of ZnO nanowires through thermal oxidation of metallic zinc films on CdTe substrates

O. Martínez[a,*], V. Hortelano[a], J. Jiménez[a], J.L. Plaza[b], S. de Dios[b], J. Olvera[b], E. Diéguez[b], R. Fath[c], J.G. Lozano[c], T. Ben[c], D. González[c], J. Mass[d]

[a] Optronlab Group, Dpto. Física Materia Condensada, Edificio I+D, Universidad de Valladolid, Paseo de Belén 1, 47011, Valladolid, Spain
[b] Laboratorio de Crecimiento de Cristales, Departamento de Física de Materiales, Facultad de Ciencias, Universidad Autónoma de Madrid, Cantoblanco, 28049 Madrid, Spain
[c] Dpto. Ciencia de los Materiales e Ingenieria Metalurgica y Q.I., Facultad de Ciencias, Apdo. 40, 11510 Puerto Real, Cádiz, Spain
[d] Dpto. de Física, Universidad del Norte, Km.5 Vía Puerto Colombia, Barranquilla, Colombia

ARTICLE INFO

Article history:
Received 2 August 2010
Received in revised form 10 February 2011
Accepted 11 February 2011
Available online 22 February 2011

Keywords:
Oxides
Zinc compounds
Semiconducting II–VI materials

ABSTRACT

⟨1 1 $\bar{2}$ 0⟩ wurtzite ZnO nanowires (NWs) have been obtained by oxidizing in air at 500 °C thermally evaporated Zn metal films deposited onto CdTe substrates. The presence of Cd atoms from the substrate on the ZnO seeding layer and NWs seems to affect the growth of the NWs. The effects of the oxidation time on the structural and optical properties of the NWs are described in detail. It is shown that the NWs density decreases and their length increases when increasing the oxidation time. Thicker Zn layers result in thinner and longer ZnO NWs. Very long oxidation times also lead to the formation of a new CdO phase which is related to the partial destruction and quality reduction of the NWs. The possible process for ZnO NW formation on CdTe substrates is discussed.

1. Introduction

Semiconducting ZnO shows interesting physical properties and represents a promising candidate for the next generation of electronic, optoelectronic and sensor devices. Amongst these properties, we can cite its wide bandgap (3.3 eV at room temperature), high exciton binding energy (60 meV), and chemical stability [1]. ZnO films deposited onto different substrates have received a great deal of attention because of its applications as transistors and diodes [2,3]. More recently, strong research efforts have been addressed towards the study of ZnO based nanoscale structures, like nanowires and nanorods [4]. This is due to their potential applications for the fabrication of ultraviolet (UV) lasers [5], nanogenerators [6], highly sensitive photodetectors, optical switches [7], etc. In addition, ZnO nanostructures are also very interesting from the fundamental point of view, as they can provide some fundamental understanding about basic optoelectronic mechanisms [8].

Research on ZnO nanostructures has been usually focused on both nanoscale and self-assembly fabrication techniques [9–11]. In this dynamic field, other topics like doping and morphology control of individual nanostructures are also of interest, since nanoscale structures are supposed to be the building blocks for the future fabrication of advanced devices such as nano-FETs, nano-LEDs, and nano-lasers [12–14]. In addition, ZnO nanostructures can be used as sensitive sensor nanodevices. Therefore, it is of primary importance to explore novel nanowire morphologies as well as their surface properties, since they have a dramatic impact in sensing applications [15–17]. Amongst all the available techniques used for the fabrication of ZnO nanostructures, the most commonly investigated ones are the metal–organic chemical vapour deposition (MOCVD), vapour phase epitaxy (VPE), direct carbo-thermal growth, and pulsed laser deposition (PLD) [18,19]. These techniques require expensive systems and severe environmental conditions, as they operate at high temperatures (~800–1400 °C) and low pressures. Therefore, other techniques are currently being explored, with the aim to produce ZnO nanostructures in a simpler way. In particular, the hydrothermal synthesis route is an important method for wet chemistry which has attracted the attention of many material chemists and has been successfully applied to the growth of ZnO nanostructures [20–23]. In this technique, an aqueous solution including a salt and a surfactant is maintained inside an autoclave at temperatures as low as 130 °C during several hours. The main advantage of this method is that it is capable to produce vertical ZnO nanowire arrays on any flat substrate that can survive heat treatments at 200 °C or greater. Nevertheless, despite the ease in implementing hydrothermal techniques, the growth rate and the optical quality (as determined by bound exciton linewidths at low temperatures) of ZnO NWs deposited in this manner is generally significantly poorer than that of NWs grown by the other

* Corresponding author. Tel.: +34 983 184956; fax: +34 983 184956.
E-mail address: oscar@fmc.uva.es (O. Martínez).

0925-8388/$ – see front matter © 2011 Elsevier B.V. All rights reserved.
doi:10.1016/j.jallcom.2011.02.063

techniques [24,25]. In addition, the size and shape of the nanoparticles are difficult to control. For these reasons there exists nowadays a trend to combine the hydrothermal synthesis with vapour phase deposition techniques, which can supply high quality optical and crystalline NWs [26].

In this work, we report on a simple technique for fabricating high quality ZnO nanowires (NWs) by oxidising in air Zn metal films deposited onto CdTe substrates. The formation of ZnO microcrystals by Zn oxidation is known from the early 50's. In 1954 Takagi [27] demonstrated for the first time the formation of ZnO microscopic needles from the oxidation of both brass (Cu 80% and Zn 20%) and Zn substrates. This technique has recently been used to grow a variety of ZnO nanostructures [28–31]. However, these interesting works are mainly based on the analysis of Zn-based substrates, and little research has been devoted to more interesting substrates like semiconductors. In particular, the combination of transparent (wide band gap) nanostructured semiconductors like ZnO NWs arrays working as n-type window layers with inorganic solar absorber materials such as CdTe provides new routes in the design of solar cell photovoltaic devices. The use of highly structured windows produces a surface enlargement and an increase of the photon path length, allowing the reduction of the absorber thickness without a loss in light absorption [32]. The association of nanostructured compounds with well-developed semiconductor substrates should give rise to cheaper solar cells with higher conversion efficiencies [33].

However, from our previous work we have concluded that the nature of the substrate seems to be determinant in order to promote the growth of the ZnO NWs. In fact, we have observed the formation of ZnO NWs in the case of using CdTe substrates. On the other hand, other substrates with the same zinc-blende structure previously used such as GaSb, did not lead to the growth of ZnO NWs, even when using similar growth conditions [34]. In this work we describe a detailed structural and compositional analysis of the parameters affecting the growth of ZnO NWs on CdTe substrates, a potential candidate for photovoltaic applications [35]. It also represents a deeper study on some preliminary results previously reported by our group [36,37]. A model of the mechanism involved in the NWs formation is also advanced. This methodology opens new possibilities for cost effective mass production of high quality ZnO NWs on alternative substrates at low temperatures.

2. Experimental details

[1 1 1] oriented CdTe single crystals were grown by the Bridgman–Stockbacker method by using a vertical furnace with an oscillation facility. The details of this technique have been reported elsewhere [38,39]. The growth took place inside high purity quartz ampoules being 30 cm long and 12 mm inner diameter. High purity Cd (7N) and Te (7N) were used as raw materials. Several wafers were cut from the CdTe crystals perpendicular to the growth axis. The wafers were polished using 0.05 μm alumina powder until mirror-like surfaces were obtained. The final dimensions of the CdTe substrates used for the growth of the ZnO films were about 12 mm × 6 mm × 1.5 mm.

ZnO films were prepared following two steps: (i) a Zn metal film layer was evaporated (at a temperature of 800 °C) on top of the CdTe substrate. The evaporation took place inside a quartz ampoule located in a horizontal furnace. Only the Zn (6N) pellets were heated, keeping the substrate close to room temperature during this evaporation step. Different deposition times, ranging from 3 to 5 min, were used. Profilometry measurements of the Zn film thickness gave values ranging from 15 to 30 μm. (ii) A further oxidation step was performed in air at 500 °C. More details of the preparation technique can be found elsewhere [34,36,37].

The effect of the oxidation time on the properties of the films was analysed on different samples. In particular, three samples, denoted as A1, A2 and A3, were prepared under the same Zn metal film deposition conditions (3 min., 800 °C) but with different oxidation times (1, 18 and 188 h, respectively). Another sample (denoted as B) was prepared with a thicker Zn film (5 min., 800 °C) and further oxidized during 20 h, in order to study also the effect of the Zn metal thickness. Table 1 resumes the deposition and oxidation parameters for the four studied samples.

High resolution scanning electron microscopy (HRSEM) analyses were carried out with a Philips SEM-FEG-XL30 microscope. Energy dispersive X-ray (EDX–SEM) analyses were performed in a SEM (Hitachi S-3000N), with an attached EDX analyser (Oxford Instruments, model INCAxsight). CL measurements (panchromatic images as well as CL spectra) were carried out at liquid nitrogen temperature (80 K) with a XiCLOne system (Gatan UK) attached to a LEO 1530-Carl Zeiss-FESEM microscope. The luminescence signal was detected with a Peltier cooled CCD. X-ray diffraction measurements were performed by means of a Siemens D-5000 diffractometer. Conventional and high resolution (HR-) transmission electron microscopy (TEM), as well as high angle annular dark field (HAADF), EDX and electron energy loss spectroscopy (EELS) in scanning-TEM (STEM) mode were carried out in cross section geometry samples using JEOL 2010F and JEOL 2011 microscopes, both working at 200 kV. For these measurements the NWs were scraped off from the substrate and then dispersed on a lacey carbon-coated copper grid.

3. Results

ZnO films were previously obtained by using the simple route of the Zn metal oxidation at atmospheric pressure [34]. In those cases, the substrates used were GaSb, and we did not observe ZnO NWs. However, ZnO NWs have been obtained when using CdTe as a substrate instead of GaSb. Low magnification SEM images of the growth sequence of sample B are shown in Fig. 1. Fig. 1a shows the Zn micro-crystals forming the Zn metal film. Fig. 1b shows the SEM image from the same sample after the oxidation step: the Zn micro-crystal shape still remains visible, but the crystals now appear covered by a dense tangle of NWs, the NWs thus appearing in the surface of the ZnO seeding layer formed after the oxidation step. The characterization was addressed towards the study of these NWs, their composition, structure and optical properties; also, a tentative scenario for the growth of these NWs will be discussed.

3.1. Influence of the growth parameters

Prior to the intensive study of the individual NWs, the influence of the growth parameters on the morphology and external shape of the NWs were studied by SEM, EDX and XRD techniques. Figs. 2 and 3 show the SEM images from the four studied samples. Samples from series A, with the same Zn deposition conditions (see Table 1), show different nanostructures as a consequence of the different oxidation times. The early stages of the NW formation are observed in sample A1, for which shorter oxidation times are used (Figs. 2a and 3a). They appear as a dense filamentary structure, with oriented thin (~60 nm) and short (<1 μm) wires. The crystalline quality of these NWs is decreased as they show a remarkable granular external aspect, Fig. 3a. The NWs form parallel straight arrays although there are flake bright contrasts along all the NWs. As the oxidation time increases, long NWs (up to several micrometres) appear. These NWs are found to be around 50–80 nm in diameter (Figs. 2b,c and 3b,c). The tangle of NWs is denser for intermediate oxidation times (sample A2, 18 h, Figs. 2b and 3b) than for very long oxidation times (sample A3, 188 h, Figs. 2c and 3c). In fact, very long oxidation times (sample A3) do not result in better NWs formation, but it seems that the NWs vanish under persistent oxidation (Figs. 2c and 3c). On the other hand, the influence of the Zn film thickness can be addressed from the comparison of samples A2 and B. Both of them were grown with similar oxidation times but with different Zn deposition times. Profilometry measurements demonstrated that the Zn film in sample B (30 μm) was twice as thicker as that of sample A (15 μm). Figs. 2b and d and 3b and d show SEM images of both samples, demostrating better NW formation (longer and thinner NWs) in sample B. Some of the nanostructures observed in this sample (B) are a few tenths of micrometres long and 10–20 nm in diameter. This clearly points out to the influence of the Zn film thickness: thicker Zn films lead to an enhanced development of the nanostructures growth during the oxidation process, at least up to 30 μm thickness.

The results of the SEM–EDX analyses are summarized in Table 1. It should be noticed that the Cd concentration (and Te) is higher, for the shortest oxidation time (sample A1). This behaviour can be

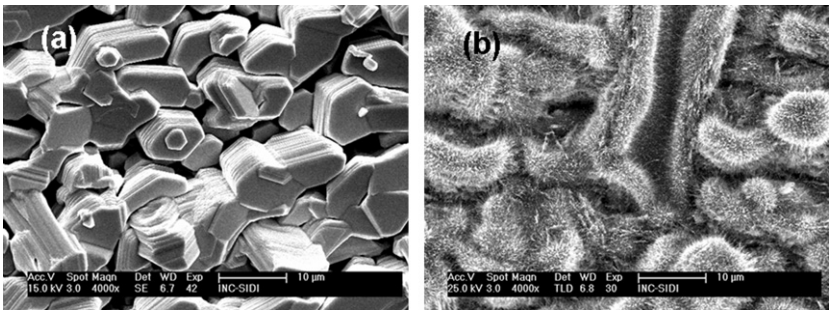

Fig. 1. SEM images from sample B, (a) before, and (b) after the oxidation step.

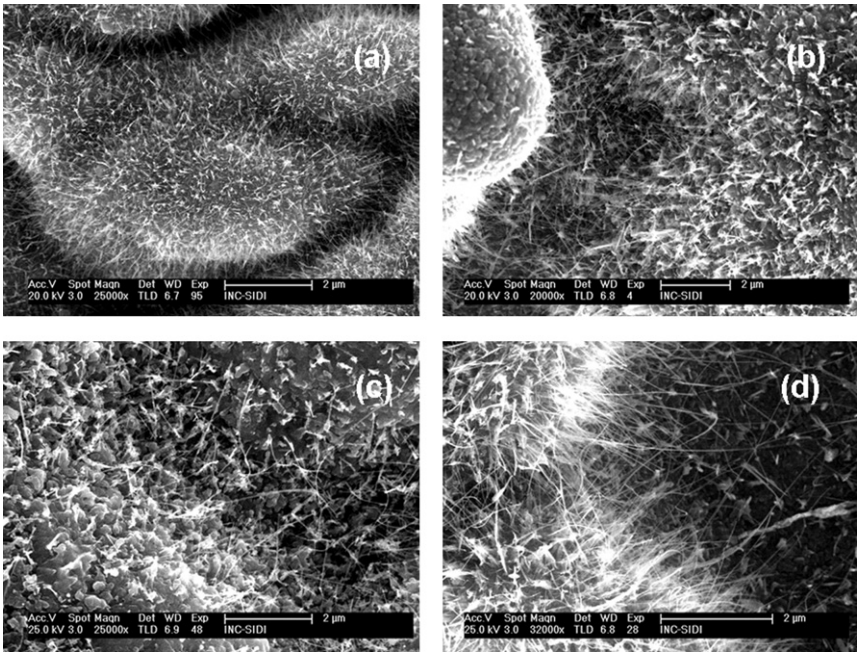

Fig. 2. SEM images of the ZnO NWs: (a) sample A1, (b) sample A2, (c) sample A3 and (d) sample B.

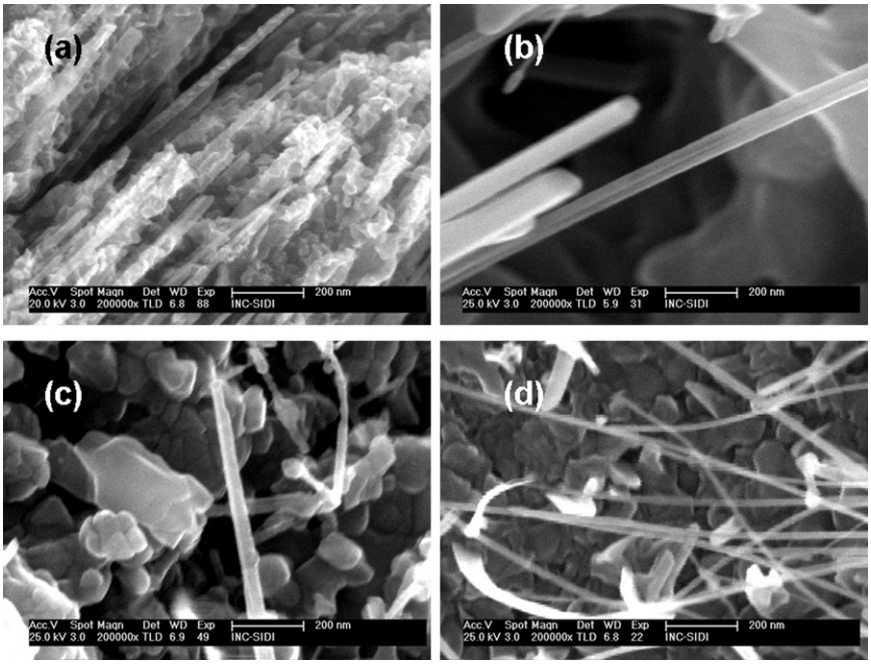

Fig. 3. Higher magnification SEM images of the ZnO NWs: (a) sample A1, (b) sample A2, (c) sample A3 and (d) sample B.

Table 1
List of samples with growth parameters and results of the EDX–SEM analyses (concentrations are in atomic %; the standard deviation values are indicated in parenthesis).

Sample	Zn metal evap. time (min.)[a]	Oxidation time (h)[b]	EDX–SEM analyses			
			Cd	Te	O	Zn
Al	3	1	4.76 (0.43)	0.19 (0.14)	57.22 (0.89)	37.84 (0.59)
A2	3	18	0.13 (0.18)	0.24 (0.12)	50.32 (0.74)	49.32 (0.67)
A3	3	188	1.18 (0.29)	0.77 (0.11)	53.01 (0.31)	45.04 (0.54)
B	5	20	0.23 (0.13)	0.19 (0.08)	46.90 (3.39)	38.67 (5.22)

[a] Zn metal evaporation temperature: 800 °C.
[b] Oxidation temperature: 500 °C.

understood considering that Cd and Te atoms might be desorbed from the back-surface of the CdTe substrate during the oxidation step (at 500 °C). They would form a Cd (and Te)-rich atmosphere in which the oxidation of the Zn film takes place (Fig. 4).

XRD measurements at a glancing angle of 1° (GA-XRD) were also carried out in order to better clarify the presence of Cd and Te (Fig. 5). It should be noted that at such glancing angle the very top surface is mainly probed. The Rietveld refinements of the detected phases have been used to estimate the compositional percentage of each one (also shown in Fig. 5). The atomic positions and the symmetry, used as starting conditions for the refinement of the different phases, are: ZnO–hexagonal *P63mc*–(Zn: 0.37, 0.63, 0; O: 0.333, 0.667 and 0.38), CdO–cubic *Fm3m*–(Cd: 0, 0, 0; O: 0.5, 0.5 and 0.5), Cd–hexagonal *P63/mmc*–(0.333, 0.667 and 0.25), Zn–hexagonal *P63/mmc*–(0.333, 0.667 and 0.25), CdTe–cubic *F-43m*–(Cd: 0, 0, 0; Te:0.25, 0.25 and 0.25) and ZnTe–cubic *F-43m*–(Zn: 0, 0, 0; Te:0.25, 0.25 and 0.25). Table 2 shows the obtained percentages, as well as the refined lattice parameters for each phase. The CdTe phase is detected only in sample A1 (Table 2). For longer oxidation times, the presence of the CdTe phase on the surface decreases, and finally disappears for the longest oxidation time. It is interesting to note also the presence of $Cd_{1-x}Zn_xTe$ secondary phases. This phase constitutes less than 1% in all samples except for sample A1. Calculations based on the refined lattice parameter-following Vegard's law – gives a phase composition $x = 0.85$: $Cd_{0.15}Zn_{0.85}Te$. The presence of this phase indicates the intermixing between Cd and Zn cations. The formation of this new phase occurred because the free energy of mixing in CdTe–ZnTe is more negative than that of the ideal solution, forming a continuous solid solution with no phase separation [40]. It is worth noting that, according to the XRD data, Cd appears also as a separate phase for all the samples (except sample A3), while Te was not detected as a separate phase (see Table 2). Sublimation in CdTe–ZnTe system is incongruent, and therefore preferential evaporation of the volatile species is expected [40]. Concerning the elements involved in our case, Cd is more volatile than Te. The fact that Te is not observed as a separate phase does not exclude its presence in the CdTe phase, thus connecting the XRD and EDX data. On the other hand, the presence of the Zn phase is only detected for sample A1, the one with the shorter oxidation time (only 1 h) – this phase is not detected or is lower than 1% in the other samples. This indicates that the oxidation of the deposited Zn metal film is not led to completion under the shortest oxidation time. In fact, it is observed that, the higher the ZnO content is, the lower the Zn metal content is measured. Finally, it was observed that the sample with the longest oxidation time presents a new CdO phase. The presence of this new phase is anti-correlated to the presence of the Cd phase, detected for samples A1, A2 and B, with much shorter oxidation times.

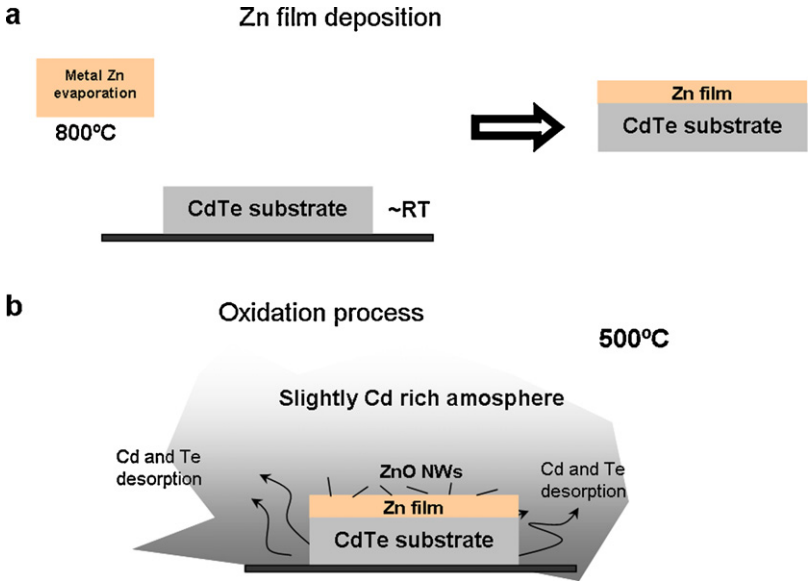

Fig. 4. Schematic representation of the two step NW growth process. (a) Zn film deposition at 800 °C (the temperature near the substrate is close to RT); (b) oxidation step in air at 500 °C, where the desorption of Cd (and in a less extend Te) atoms from the back-surface of the substrate leads to a slightly Cd rich atmosphere.

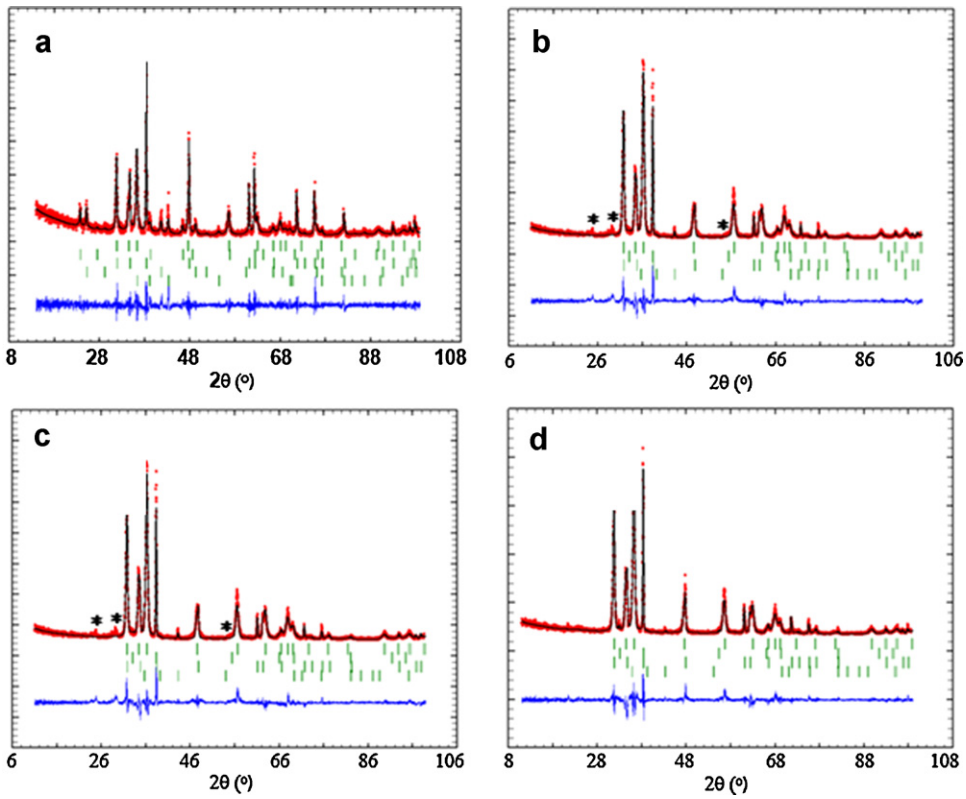

Fig. 5. GA-XRD spectra of the ZnO films: (a) sample A1, (b) sample A2, (c) sample A3 and (d) sample B. The Rietveld analysis is also shown.

3.2. Structure of the individual NWs

To confirm the composition and the structure of the NWs, we have carried out a study of the individual NWs by means of the HRTEM technique, as well as by HAADF, EDX and EELS analysis in STEM mode. Fig. 6a shows a TEM image of some NWs in sample B, scrapped off from the substrate and spread on a lacey carbon film in a Cu grid. The NWs show a very straight shape with regular diameter between 15 and 25 nm, ending in a more bulky head; there are no evidences of structural defects such as planar defects [41] or dislocations inside the NWs, thus displaying a high structural quality. The entire NWs exhibit a homogeneous contrast, in agreement with the HAADF analysis. These data indicate that the NWs have a uniform composition, both in longitudinal and transversal directions; they also indicate that there is no presence of different phases or precipitates at the nanometric scale. Furthermore, the EELS and EDX analyses also show that the NWs are constituted mainly by Zn and O, although low signals from Cd and Te also appear in the EDX spectra. In particular, Cd, with a very low atomic percentage composition (lower than 2%), becomes visible in the NWs. Cadmium is found in the root of the NWs and in the bottom lower trunk section, but not in the top. These data confirm the presence of Cd atoms on the ZnO seeding layer and its incorporation to the bottom of the NWs (as indicated also by the XRD data). Cd atoms likely influence the further development of the ZnO NWs. The role that Cd atoms might play should be searched beyond of a merely catalyst located in the end of the NW, since we have not found Cd signal neither in the head nor in the top of the NWs.

Fig. 6b shows a HRTEM image of a NW (sample B) taken along the [0 0 0 1] pole. From the images and their Fast Fourier transforms (inset in Fig. 6b), the measured distance between lattice planes is 0.26 nm, which is unambiguously related to the wurtzite phase of ZnO. The NWs grow along the $[1\ \ 1\ \ \bar{2}\ \ 0]$ direction, being $(0\ 0\ 0\ 1)$ its top/bottom planes and $(0\ \ \bar{1}\ \ \bar{1}\ \ 0)$ the lateral ones.

Table 2
Compositional data deduced from GA-XRD Rietveld analysis (the standard deviation values are indicated in parenthesis).

Phases	ZnO	CdTe	CdZnTe	CdO	Cd	Zn
Samples						
	65(1) %	4.9(1) %	9.7(7) %	n.d.[a]	11.3(2) %	9.7(7) %
Al	a = 3.2542(4)	a = 6.4SS(l)	a = 6.135(1)		a = 2.9800(2)	a = 2.6677(9)
	c = 5.201(1)				c = 5.619S(3)	c = 4.934(5)
	88.0(7) %	<1%		<1%	10.3(1) %	<1%
A2	a = 3.2541(2)			a = 4.700(7)	a = 2.980(1)	a = 2.6540(9)
	c = 5.2089(5)				c = 5.6223(4)	c = 5.041(5)
	92(1) %	<1%		7.1(5) %	<1%	n.d.
A3	a = 3.2541(2)			a = 4.700(7)	a = 2.980(1)	
	c = 5.2089(5)				c = 5.6223(4)	
	83.1(6) %	n.d.		<1%	15.6(2) %	<1%
B	a = 3.2524(2)			a = 4.697(l)	a = 2.9797(l)	a = 2.6554(2)
	c = 5.2037(4)				c = 5.6244(4)	c = 5.0218(3)

[a] n.d., non detected.

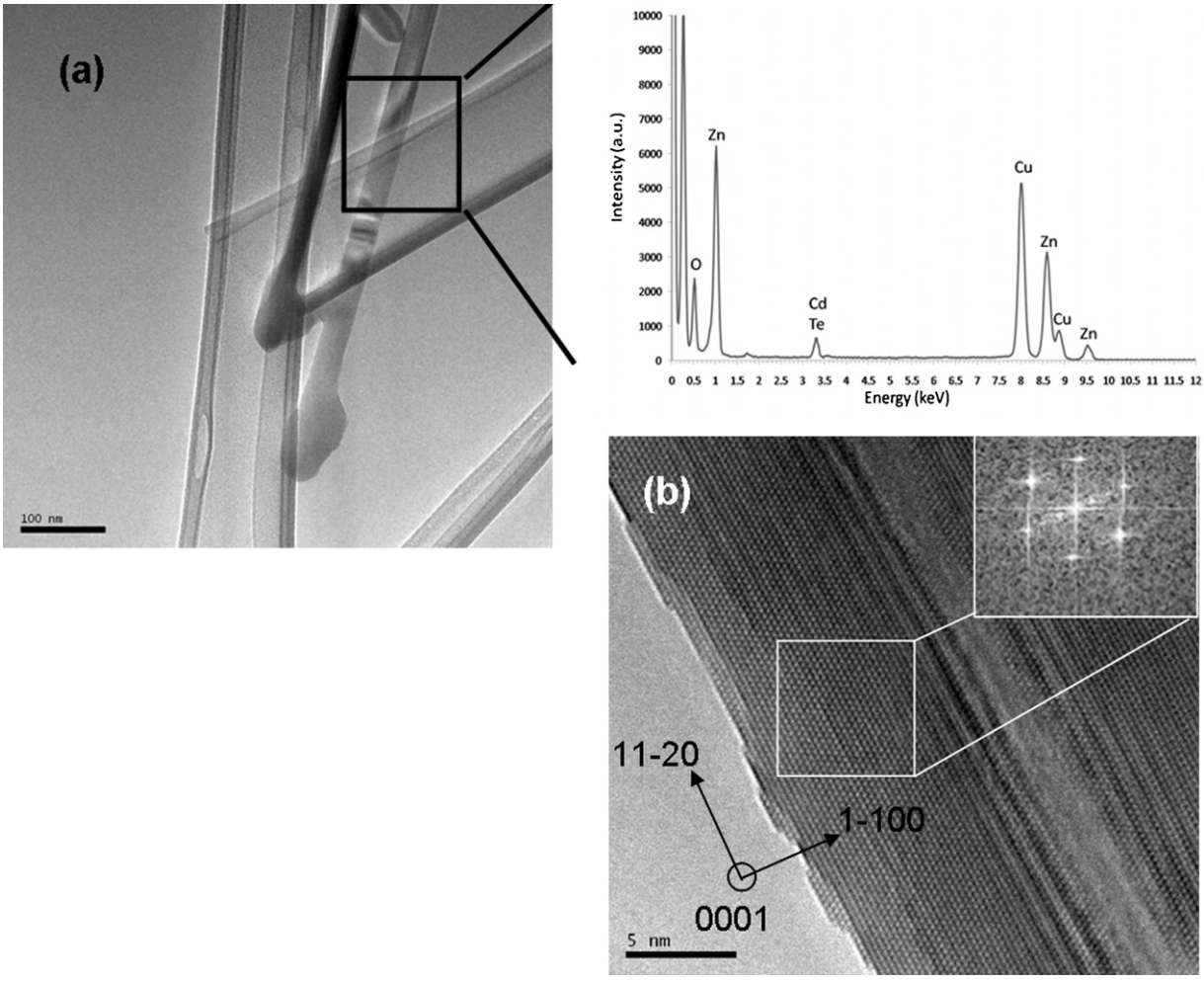

Fig. 6. (a) TEM image and EDX spectrum of a NW from sample B. The NW is mainly set up by ZnO, although Cd appears at low content. (b) HRTEM image of a NW; the inset shows, for the selected region, the corresponding Fast Fourier transform.

The growth direction can be associated with differences in surface energies amongst (0 0 0 1), {0 $\bar{1}$ $\bar{1}$ 0} and {2 $\bar{1}$ $\bar{1}$ 0}. In fact, due to the differences in surface energies, freestanding nanowires of ZnO are usually dominated by the lower energy, non-polar surfaces, such as {0 $\bar{1}$ $\bar{1}$ 0} and {2 $\bar{1}$ $\bar{1}$ 0}, with growth directions parallel to [0 0 0 1] [42]. According to our data, our NWs maximize the polar (0 0 0 1) facets, which can be explained only by changes in the relative surface activities of the growth facets under our growth conditions. Thus, we postulate that the Cd inclusion in the ZnO NWs stabilizes the (0 0 0 1) faces, developing into a three-dimensional object with well-defined, lateral low-index crystallographic (0 $\bar{1}$ $\bar{1}$ 0) and (0 0 0 1) faces.

3.3. Optical characterization

The samples were analysed by the CL-SEM technique, very suitable to study the optical signature of the NWs. Fig. 7a and b shows SEM and panCL images, respectively, of sample B. The NWs have distinguishable luminescence, different from the luminescence of the seeding layer. Fig. 7c shows the CL spectra obtained on a NW and out of it. The main emission band is located in the UV in both cases, corresponding to the near band edge (NBE) emission. An important luminescence enhancement of the UV band in the NWs respect to the outside is observed, well correlated to the panCL image that shows bright contrast for the NWs. A broad visible band is only clearly observed outside the NWs, being its intensity nearly zero

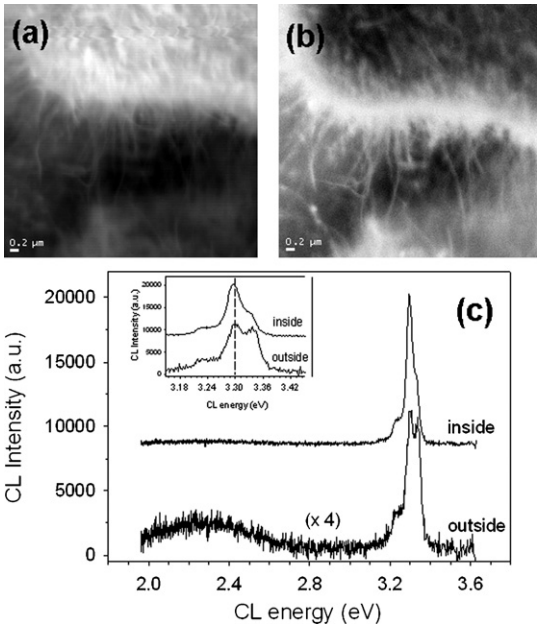

Fig. 7. (a) SEM, (b) panCL images of sample B, showing several NWs and (c) CL spectra outside and inside a NW (the inset shows an enlarged view of the NBE spectral range).

in the NWs. These data indicates the good optical properties of the ZnO NWs obtained by our growth method.

The NBE band shows three contributions, at ~3.329, 3.294 and 3.224 eV, the last two being separated by nearly the LO phonon energy in ZnO (~72 meV), thus corresponding to a DAP transition and its phonon replica [43]. The emission at ~3.329 eV is increased in the NW, and slightly shifted to the red (see the inset in Fig. 7c). Recently, surface related transitions around this energy have been observed in other ZnO NWs [44]. The increase of this emission in the NWs would be coherent with this assignment. The slightly red shift in the NWs could be also related to the Cd detected by TEM in the NWs, which would lead to a CdZnO alloyed NW.

4. Discussion

The fact that ZnO NWs were not formed on GaSb substrates under the same growth conditions [34] seems to claim for the influence of the CdTe substrate, and thus on the role of Cd or Te elements, on the formation of the NWs. The migration of Cd and Te from the substrate is postulated to happen during the oxidation step, since during the deposition of the Zn metal film the substrate does not increase its temperature (see Fig. 4). Moreover, the oxidation temperature of 500 °C is higher that the melting point of Zn (419.53 °C) which suggests that Zn liquid phase is involved in the NW nucleation (in fact, we have observed that lower oxidation temperatures do not lead to NW formation). Thus, one can expect that the oxidation process takes place in a local atmosphere slightly rich in Zn and Cd (and, to a less extent, in Te, because of its lower volatility). The formation of a Cd–Te atmosphere is possible specially under vacuum conditions, a procedure that has been used to grow CdTe films on mildly heated (200 °C) substrates under evaporation temperatures ranging from 400 to 510 °C [45]. In our case, the oxidation is carried out at atmospheric pressure, where the different vapour pressures for both components (1 kPa for Cd and 100 Pa for Te [46]) at the oxidation temperature of 500 °C ensure a slightly higher Cd enrichment of the local atmosphere.

XRD data and TEM analysis, have demonstrated the presence of Cd (and Te elements in a very low quantity) in the surface of the ZnO seeding layer and in the bottom of the NWs. Based on these results we postulate that Cd have a relevant role in the NW growth. The Cd hexagonal phase might be beneficial for the NW growth. Moreover, Cd, as a separate phase, is detected for short and medium oxidation times, when the NWs grow longer and with a higher density, as deduced by the SEM images. Nevertheless, after very long oxidation times (sample A3) Cd is not detected anymore, while a new CdO phase appears. This indicates that Cd is being oxidized for such long times. This is coherent with the fact that the more active metal, Zn, is more easily oxidized, and must oxidize nearly completely before the less active metal, Cd, does. Therefore, the Zn layer seems to work as a sacrificial anode layer, protecting Cd from oxidation. The loss of Cd phase (and/or the presence of CdO) and the destruction and impoverishment of the quality of the NWs for very long oxidation times (sample A3) seem to be correlated. This could be also at the origin of the better NW formation (in terms of longer and thinner NWs) on sample B if one assumes that a higher Zn thickness would prevent the Cd from oxidising.

The above data lead us to propose the following growth scenario: for low and intermediate oxidation times, Zn melts at the surface forming drops that act as seeds in the NW formation. The presence of hexagonal Cd phases, which migrated from the back-surface of the substrate, benefits the formation of $\langle 1\ 1\ \bar{2}\ 0 \rangle$ ZnO NWs, which further developed as the oxidation time increases. That growth takes place through a vapour–solid (VS) mechanism, in which the liquid phase is involved only in the nucleation and the vapour feeds the growth [47]. Inner Zn metal partially melts and vaporizes, forming a Zn atmosphere. During this stage, Zn works as a sacrificial anode layer protecting the Cd metal for oxidation. For very long oxidation times, all the Zn metal is exhausted, the Zn vapour pressure drops and the role of the Zn layer as a sacrificial anode ends. Cd atoms start to be also oxidized, forming a new cubic CdO phase. The formation of a CdO phase implies the collapse of Zn metal supplies and the end of the NW growth. The lower quality of the ZnO NWs could be just due to the aggregation and accumulation of the ZnO NWs for very long oxidation times, a fact that could be stimulated by the presence of the new cubic CdO phase. The exact role of the Cd element in the ZnO growth is difficult to be ascertained at the present, but it could be related to the nucleation and the stabilization of the (0 0 0 1) faces observed in the NWs. Further work is being developed to understand this point.

Finally, the method supposes a novel tool for the production of $\langle 1\ 1\ \bar{2}\ 0 \rangle$ ZnO NWs on CdTe substrates. While the conventional synthesis methods require expensive systems and rigid environmental conditions, especially high temperatures (~800–1400 °C) and low pressures, the described methodology lies in the low range of temperatures and is carried out at atmospheric pressures. The luminescence of our NWs indicates that they are promising candidates for optoelectronic nanodevices. The very small amount of Cd detected in the NWs could have a doping effect on them. In fact, a slightly red shift in the luminescence emission has been detected in the NWs. Some other effects on the optical and electrical properties could not be excluded. This is a matter of further study. In fact, we are at the beginning of the understanding of the growth formation mechanism, with many parameters which still have to be optimized. Further work is now in progress to clarify both the driving force for the growth of the NWs, and the influence that the Cd and CdO phases have on the ZnO NWs growth.

5. Conclusions

$\langle 1\ 1\ \bar{2}\ 0 \rangle$ ZnO NWs have been grown by means of a very simple method consisting on depositing a Zn metal film on top of a CdTe substrate and a further oxidation step in air at 500 °C. The NW growth occurs through a vapour–solid mechanism although the Cd migration from the substrate is postulated to be beneficial for the growth of the NWs. The growth parameters have been shown to affect both the dimensions and characteristics of the NWs. Thick Zn films and intermediate oxidation times of ~20 h lead to the best formation of the NWs, with dimensions of 10–30 nm in width an some tens of μm in length. Very long oxidation times lead to the formation of a new CdO phase affecting the good structural quality of the NWs. The NWs exhibit distinguishable optical signatures, with an enhanced UV band and reduced visible emissions with respect to the background ZnO layer.

Acknowledgments

One of the authors (J. L. P.) thanks the Spanish "Ministerio de Educación y Ciencia" for Funding through an I3 Program. We also thank the partial support of this work by Spanish Projects MAT 2007-63617, MAT2007-60643, MAT2010-15206 and MAT2007-66741-C02-02.

References

[1] Ü. Özgür, Y. Alivov, C. Liu, A. Teke, M. Reshchikov, S. Dogan, V. Avrutin, S. Cho, H. Morkoc, J. Appl. Phys. 98 (2005) 041301.
[2] J. Kim, B. Ahn, C. Lee, K. Jeon, H. Kang, S. Lee, J. Appl. Phys. 100 (2006) 113515.
[3] H. Kang, B. Ahn, J. Kim, G. Kim, S. Lim, H. Chang, S. Lee, Appl. Phys. Lett. 88 (2006) 202108.
[4] M.S. Xue, W. Li, F.J. Wang, J.S. Lu, J.P. Yao, J. Alloys Compd. 502 (2010) 127.
[5] M. Huang, S. Mao, H. Feick, H. Yan, Y. Wu, H. Kind, E. Weber, R. Russo, P. Yang, Science 292 (2001) 1897.
[6] Z. Wang, J. Song, Science 312 (2006) 242.
[7] H. Kind, H. Yan, B. Messer, M. Law, P. Yang, Adv. Mater. 14 (2002) 158.

[8] Q. Li, T. Gao, Y. Tang, T. Wang, Appl. Phys. Lett. 86 (2005) 123117.
[9] T. Chung, L. Luo, Z. He, Y. Leung, I. Shafiq, Z. Yao, S. Lee, Appl. Phys. Lett. 91 (2007) 233112.
[10] B. Zhang, N. Binh, K. Wakatsuki, Y. Segawa, Y. Yamada, N. Usami, M. Kawasaki, Appl. Phys. Lett. 84 (2004) 4098.
[11] F. He, Y. Zhao, Appl. Phys. Lett. 88 (2006) 193113.
[12] B. Xiang, P. Wang, X. Zhang, S. Dayeh, D. Aplin, C. Soci, D. Yu, D. Wang, Nano. Lett. 7 (2007) 323.
[13] J. Johnson, K. Knutsen, H. Yan, M. Law, Y. Zhang, P. Yang, R. Saykally, Nano. Lett. 4 (2004) 197.
[14] X. Zhou, T. Sham, Y. Shan, X. Duan, S. Lee, R. Rosenberg, J. Appl. Phys. 97 (2005) 104315.
[15] Y. Cui, Q. Wei, H. Park, C. Lieber, Science 293 (2001) 1289.
[16] L. Liao, H. Lu, J. Li, C. Liu, D. Fu, Y. Liu, Appl. Phys. Lett. 91 (2007) 173110.
[17] G. Zheng, F. Patolsky, Y. Cui, W. Wang, C. Lieber, Nat. Biotechnol. 23 (2005) 1294.
[18] J. Son, S. Lim, J. Cho, W. Seong, H. Kim, Appl. Phys. Lett. 93 (2008) 053109.
[19] M. Willander, O. Nur1, Q. Zhao, L. Yang, M. Lorenz, B. Cao, J. Zúñiga-Pérez, C. Czekalla, G. Zimmermann, M. Grundmann, A. Bakin, A. Behrends, M. Al-Suleiman, A. El-Shaer, A. Che-Mofor, B. Postels, A. Waag, N. Boukos, A. Travlos, H. Kwack, J. Guinard, D. Le Si Dang, Nanotechnology 20 (2009) 2001.
[20] J. Yang, J. Zheng, H. Zhai, X. Yang, L. Yang, Y. Liu, J. Lang, M. Gao, J. Alloys Compd. 489 (2010) 51.
[21] Z. Lockman, Y.P. Fong, T.W. Kian, K. Ibrahim, K. Abdul Razak, J. Alloys Compd. 493 (2010) 699.
[22] S. Xu, Y. Ding, Y. Wei, H. Fang, Y. Shen, A.K. Sood, D.L. Polla, Z.L. Wang, J. Am. Chem. Soc. 131 (2009) 6670.
[23] M. Wang, Z. Xu, L. Ge, E.J. Kim, S.H. Hahn, J. Yang, X. Cheng, J. Alloys Compd. 507 (2010) L21–L25.
[24] Q.X. Zhao, L.L. Yang, M. Willander, B.E. Sernelius, P.O. Holtz, J. Appl. Phys. 104 (2008) 073526.
[25] R.T.R. Kumar, E. McGlynn, M. Biswas, R. Saunders, G. Trolliard, B. Soulestin, J.R. Duclere, J.P. Mosnier, M.O. Henry, J. Appl. Phys. 104 (2008) 084309.
[26] D. Byrne, E. McGlynn, K. Kumar, M. Biswas, M.O. Henry, G. Hughes, Cryst. Growth Des. 10 (2010) 2400.
[27] R. Takagi, J. Phys. Soc. Jpn. 9 (1955) 162.
[28] H. Dang, J. Wang, S. Fan, Nanotechnology 14 (2003) 738.
[29] R. Kyoung, H. Jang, C. Kim, J. Ceram. Soc. Jpn. 113 (2005) 337.
[30] Y. Gui, C. Xie, Q. Zhang, M. Hu, J. Yu, Z. Weng, J. Cryst. Growth 289 (2006) 663.
[31] M. Zha, D. Calestani, A. Zappettini, R. Mosca, M. Mazzera, L. Lazzarini, L. Zanotti, Nanotechnology 19 (2008) 325603.
[32] K. Ernst, A. Belaidi, R. Könenkamp, Semicond. Sci. Technol. 18 (2003) 475.
[33] R. Tena-Zaeraa, A. Kattya, S. Bastidea, C. Lévy-Clémenta, B. O'Reganb, V. Muñoz-Sanjosé, Thin Solid Films 483 (2005) 372.
[34] O. Martínez, J.L. Plaza, J. Mass, B. Capote, E. Diéguez, J. Jiménez, Superlattices Microstruct. 42 (2007) 145.
[35] A. Bosio, N. Romeo, S. Mazzamuto, V. Canevari, Prog. Cryst. Growth Charact. Mater. 52 (2006) 247.
[36] J.L. Plaza, O. Martínez, V. Carcelén, J. Olvera, L.F. Sanz, E. Diéguez, Appl. Surf. Sci. 254 (2008) 5403.
[37] J.L. Plaza, O. Martínez, S. de Dios, J. Olvera, E. Diéguez, J. Cryst. Growth 312 (2010) 64.
[38] V. Corregidor, V. Babentsov, J.L. Castaño, M. Fiederle, T. Feltgen, K. Benz, E. Diéguez, J. Mater. Res. Soc. 17 (2002) 3037.
[39] J.L. Plaza, P. Hidalgo, B. Méndez, J. Piqueras, J.L. Castaño, E. Diéguez, J. Crys. Growth 198–199 (1999) 379.
[40] A. Alikhanian, V. Guskov, J. Greenberg, M. Fiederle, K. Benz, J. Alloys Compd. 371 (2004) 82.
[41] Y. Ding, X. Kong, Z. Wang, Phys. Rev. B 70 (2004) 235408.
[42] Z. Wang, Mater. Sci. Eng. R 64 (2009) 33.
[43] B. Zhang, N. Binh, K. Wakatsuki, Y. Segawa, Y. Kashiwaba, K. Haga, Nanotechnology 15 (2004) S382.
[44] J. Reparaz, F. Guell, M. Wagner, A. Hoffmann, A. Cornet, J.R. Morante, Appl. Phys. Lett. 96 (2010) 053105.
[45] A. Ali, N. Shah, A. Aqili, A. Maqsood, Cryst. Growth Des. 6 (2006) 2149.
[46] A. Ubelis, J. Eng. Phys. Thermophys. 42 (1982) 309.
[47] L. Zanotti, M. Zha, D. Calestani, E. Comini, G. Sberveglieri, Cryst. Res. Technol. 40 (2005) 932.